Available online at www.sciencedirect.com

ScienceDirect

Advances in Space Research 63 (2019) 4003–4014

ADVANCES IN SPACE RESEARCH (a COSPAR publication)

www.elsevier.com/locate/asr

Ionospheric *f*oF2 disturbance forecast using neural network improved by a genetic algorithm

Jun Zhao [a,*], Xiaojun Li [a], Yi Liu [b], Xiang Wang [b], Chen Zhou [b,*]

[a] China Research Institute of Radiowave Propagation, Qingdao 266107, China
[b] Department of Space Physics, School of Electronic Information, Wuhan University, Wuhan, Hubei 430072, China

Received 2 August 2018; received in revised form 26 February 2019; accepted 28 February 2019
Available online 6 March 2019

Abstract

A single station short-term ionospheric disturbance forecasting model has been developed with a genetic algorithm-based neural network (GA-NN). The genetic algorithm is used to optimize the initial weights of the neural network to avoid the local minimum during NN training. Using this model, the single station predictions of the ionospheric F2 layer critical plasma frequency, *f*oF2, with the time-scale 1–24 h in advance in the China region have been investigated. Input parameters of the forecasting GA-NN model include the Beijing time (GMT+8), season information, solar zenith angle, day number, solar activity, geomagnetic activity, neutral winds, geographic coordinates and previous values of *f*oF2. The training dataset in this model are obtained from the ionosonde stations in China. The data coverage is from 1990 to 2004 (more than one solar cycle) except 1995 and 2000. The data of ionospheric disturbances in 1995 (solar minimum) and 2000 (solar maximum) are used as the validation dataset. The prediction results at the different stations show that 1 h ahead prediction is more accurate than predictions of 3, 6, 12 and 24 h ahead. Comparisons between the observed and predicted values of *f*oF2 in the low and middle latitudes during the year of solar minimum (1995) and solar maximum (2000) indicate that, the prediction accuracy at middle latitudes are generally better than that at low latitudes. The prediction root-mean-square error (RMSE) in the low solar activity is smaller than that in the high solar activity. The ionospheric disturbances prediction results manifest that the model works well even when the observed values of *f*oF2 are far away from the monthly median value and the ionospheric storm lasts for 18 h.

Keywords: Ionospheric disturbance; *f*oF2; Forecasting; Neural network; Genetic algorithm

1. Introduction

The Earth's ionosphere has evident day-to-day variability. Ionospheric day-to-day variability can be related to solar activity, geomagnetic activity and large-scale lower atmospheric waves. Ionospheric day-to-day variability is a critical factor for ionospheric prediction.

The most significant source for the day-to-day variability is the ionospheric storm, which can be considered as geomagnetic sources comparing to meteorological sources. An ionospheric storm is an extreme phenomenon of space weather. An ionospheric storm has evident effects on ground- and space-based electronic systems, including damages of electric power systems, atmospheric drag force on satellites, GNSS positioning error, HF communication interruption, and disruption of UHF satellite links (Buonsanto, 1999). Therefore, it is very important to quantitatively forecast the ionospheric storm. Much work so far has focused on the geomagnetic and ionospheric storms in the last few decades (Abdu et al., 1995; Cander and Mihajlovic, 2005; Hebden et al., 2005). Moreover, many modelling techniques have been attempted to forecast the

* Corresponding authors.
E-mail addresses: zhaojunxinxiang@qq.com (J. Zhao), chenzhou@whu.edu.cn (C. Zhou).

https://doi.org/10.1016/j.asr.2019.02.038
0273-1177/

ionospheric storms (Zolesi and Cander, 2000; Bilitza, 2002). The Earth's ionosphere is a complex nonlinear system, while the neural network (NN) is a data-driven nonlinear model. Therefore, artificial neural network has been employed to build suitable forecasting models to predict the ionospheric *f*oF2 (Ban et al., 2011).

The F2 layer critical plasma frequency, *f*oF2, is one of the most important ionospheric parameters (Oyeyemi et al., 2006; Goodman, 1992). Many researchers have extensively explored the forecast of the ionospheric *f*oF2 variability for short terms (hourly) by using the neural network. For instance, models for ionospheric *f*oF2 1 h ahead (Altinay et al., 1997; Poole and Mckinnell, 2000), 1–5 h ahead (Oyeyemi et al., 2005b) and 1–24 h ahead (Wintoft and Cander, 2000; Nakamura et al., 2007) predictions have been developed before. Wintoft and Cander (1999) used a delay neural network for the short-term forecast of the ionospheric parameter *f*oF2. Francis et al. (2000) have adopted the nonlinear radial basis function (RBF) neural networks (NNs) to improve the prediction accuracy of the ionospheric parameters of hourly, daily, and monthly timescales.

As the general back propagation (BP) neural network (NN) is based on gradient descent principle, gradient search techniques tend to get trapped at local minimum. The performance degradation appears due to the fact that the solution complex spaces have nearly global minima which are sparse among the local minima (Montana and Davis, 1989). Thus, the back propagation (BP) neural network (NN) is easy to fall into the local minimum in the learning phase, not offering the globally optimal solution (Montana and Davis, 1989). In this work, a genetic algorithm (GA) (Lampinen, 2003; Renner and Ekárt, 2003) is adopted to optimize the initial weights of the neural network to avoid the local minimum phenomenon (Wang et al., 2013; Zhou et al., 2013).

In this study, a single station short-term ionospheric disturbance forecasting model is developed with a genetic algorithm-based neural network (GA-NN). By using this model, the single station prediction of *f*oF2 with timescales of 1–24 h ahead in the China region are investigated. We also focus on the prediction of *f*oF2 during the ionospheric storm period. The prediction results for 1, 3, 6, 12 and 24 h ahead at the different ionosonde stations are presented in this paper. We compare the results between the low and middle latitudes during the high and low solar activity periods. In addition, specific cases are shown to illustrate the prediction performance of the model.

The purpose of this paper is to evaluate the performance of the GA-NN ionospheric disturbance forecasting model. In Section 2, we present the description of ionospheric disturbance forecasting model. The input and output parameters of the model are shown in Section 3. Section 4 provides the data set and we illustrate and analyze the prediction results in Section 5. Finally, the discussion and conclusions are given in Section 6.

2. Model for *fo*F2 disturbance prediction

2.1. Method description

The typical back propagation neural network (BP NN) is based on the gradient descent principle. Usually, when the nearly global minimum is hidden among the 'local minimum', the general BP NN stops working and consequently outputs wrong results (Wang et al., 2013). To avoid the 'local minimum', we optimize the BP NN by GA, which is a model based on the biological evolution process of natural selection and genetic mechanism, and searches optimal solution by simulating the natural evolution process. The neural network improved by genetic algorithm (GA-NN) is mainly to use genetic algorithm to optimize the initial weights of the neural network and be able to better predict the output function (Goldberg et al., 1989). The specific optimization steps are described in Wang et al. (2013).

2.2. Error analysis

In order to evaluate the prediction results obtained by the GA-NN model, the prediction performances are calculated by the root mean square error (RMSE) and percent deviation *r*. The correlation coefficient ρ is used to evaluate the correlation of predicted values and the observed values. The definitions of RMSE, *r* and ρ are given by,

$$\mathrm{RMSE} = \sqrt{\frac{1}{n}\sum_{i=1}^{n}\left(f_{\mathrm{obs}i} - f_{\mathrm{pre}i}\right)^2} \tag{1}$$

$$r = \frac{1}{n}\sum_{i=1}^{n}\frac{\left|f_{\mathrm{obs}i} - f_{\mathrm{pre}i}\right|}{f_{\mathrm{obs}i}} \times 100 \tag{2}$$

$$\rho = \frac{\sum_{i=1}^{n}\left(f_{\mathrm{pre}i} - \overline{f_{\mathrm{pre}}}\right)\left(f_{\mathrm{obs}i} - \overline{f_{obs}}\right)}{\sqrt{\sum_{i=1}^{n}\left(f_{\mathrm{pre}i} - \overline{f_{\mathrm{pre}}}\right)^2}\sqrt{\sum_{i=1}^{n}\left(f_{\mathrm{obs}i} - \overline{f_{\mathrm{obs}}}\right)^2}} \tag{3}$$

where $f_{\mathrm{obs}i}$ and $f_{\mathrm{pre}i}$ are the observed value and predicted value, respectively. $\overline{f_{\mathrm{obs}}}$and $\overline{f_{\mathrm{pre}}}$ are the average of the observed and predicted values, respectively. *n* is the total number of samples.

3. Input and output parameters

The ionospheric variability depends on latitude, season and local time (Buonsanto, 1999). The input parameters of the ionospheric *f*oF2 forecasting model include three parts: (1) local time, seasonal information and day number. (2) the correlation of storm-time, the solar activity and the magnetosphere activity. (3) the values of *f*oF2 in the past hours. The input parameters are shown as below in details.

3.1. The ionosphere information

3.1.1. Diurnal variation

Studies have shown that the occurrence of the ionospheric storms are related to geomagnetic storms, and depended on the local time (*LT*) (Kirby et al., 1936; Wintoft and Cander, 2000). In this work, the Beijing Time (*BJT*, *GMT+8*) in the range of 1–24 is used to describe the diurnal variation. To keep numerical continuity and uniqueness at the midnight boundary between 2400 and 0100 *BJT* (Poole and McKinnell, 2000), we convert *BJT* to sine component (*BJTS*) and cosine component (*BJTC*), and express as,

$$BJTS = \sin\left(\frac{2\pi \times BJT}{24}\right) \tag{4}$$

$$BJTC = \cos\left(\frac{2\pi \times BJT}{24}\right) \tag{5}$$

3.1.2. Seasonal variation

Season information has important effects on the evolution of ionospheric storm (Appleton et al., 1937; Oyeyemi and Poole, 2004). The *fo*F2 shows similar characteristics in spring and fall. There are also some similarities between the two successive seasons. However, the characteristics of *f*oF2 in summer and winter are different, even opposite (Tulunay et al., 2004). Table 1 shows the GA-NN inputs representing season information according to the characteristics of the seasonal variation in most area of China. To avoid the calculation trouble in NN training, we use 0.99 instead of 1 in Table 1 (Wang et al., 2013). In Table 1, take the winter input as an example, the characteristics of *f*oF2 in winter and summer are opposite, with the value of 0.99 and −0.99, respectively. Similarly, in winter, the summer input and the winter input are opposite.

The seasonal variation of the F2 layer is also related to the solar zenith angle. Thus, the solar zenith angle is considered as an input parameter. The solar zenith angle (*CHI*) with respect to each geographical location is generated by using the following expression (Oyeyemi et al., 2006):

$$\cos(x) = \sin(lat)\sin(\delta) + \cos(lat)\cos(\delta)\cos(\lambda - lon) \tag{6}$$

where *lat* is the geographic latitude; *lon* is the geographic longitude;$\delta = 23.45[\frac{360}{365}(N + 284)]$ is the sub-solar latitude, and N is the day number of the year;$\lambda = 15H - 180^{\circ}$ is the sub-solar longitude, and H is the hour number of the day. Similar to *BJT*, the solar zenith angle is converted to sine (*CHIS*) and cosine (*CHIC*) components according to:

$$CHIS = \sin\left(\frac{2\pi \times CHI}{360}\right) \tag{7}$$

$$CHIC = \cos\left(\frac{2\pi \times CHI}{360}\right) \tag{8}$$

Table 1
The GA-NN inputs of season information.

Season	Winter input	Spring input	Summer input	Fall input
Winter	0.99	0.40	−0.99	0.70
Spring	0.40	0.99	0.60	0.80
Summer	−0.99	0.60	0.99	0.40
Fall	0.60	0.80	0.40	0.99

3.1.3. Day number

The previous studies shown that, day number (*DN*) also has an effect on the variations of *f*oF2 (Williscroft and Poole, 1996; Kumluca et al., 1999). To avoid unrealistic discontinuities between 31 December (day number 365) and 1 January (day number 1), the day number is decomposed into two orthogonal vectors (*DNS* and *DNC*),

$$DNS = \sin\left(\frac{2\pi \times DN}{365}\right) \tag{9}$$

$$DNC = \cos\left(\frac{2\pi \times DN}{365}\right) \tag{10}$$

3.2. Correlation factors

3.2.1. Solar activity

The solar activity has a strong relationship with *f*oF2 (Wintoft and Cander, 2000), and the effect of the 27-day solar cycle in the ionosphere has been investigated (Apostolov et al., 2004; Liang et al., 2008). Therefore, the 27-day running mean of solar radio flux *F10.7 cm* ($F10.7_{27m}$) has been used as an input parameter in the present model.

3.2.2. Geomagnetic activity

The geomagnetic index $ap(\chi)$ is also adopted to represent the geomagnetic activity. The index $ap(\chi)$ is based on a time weighted accumulation series derived from the geomagnetic planetary index *ap*. The 33 h of integral defined as,

$$ap(\chi) = (1-\chi)[ap_0 + (\chi)ap_{-1} + (\chi^2)ap_{-2} + ...] \tag{11}$$

where χ is a persistence factor of attenuation multiplier ranging from 0 to1, with $\chi = 0.8$ in this study; ap_0 is the initial value of the magnetic index, ap_{-1}, ap_{-2} ... ap_{-11} denote values of the 3 h before, 6 h before and 33 h before.

The geomagnetic index *Dst* has a strong correlation with *f*oF2 at low latitudes (Wang et al., 2008), and the *Kp* have a strong correlation with *f*oF2 at middle latitudes (Kutiev and Muhtarov, 2001). Therefore, similar to $ap(\chi)$, we adopt $Dst(\tau)$ and $K_f(t)$ as the input parameters, and define as,

$$Dst(\tau) = (1-\tau)[Dst_0 + (\tau)Dst_{-1} + (\tau^2)Dst_{-2} + ...] \tag{12}$$

$$K_f(t) = \left(\exp\frac{1}{T} - 1\right)\sum_{\tau=-\infty}^{t-1}(Kp^2(\tau) - K_{qm}(\tau))\exp\left(-\frac{\tau - t}{T}\right) \tag{13}$$

where t is the current time; τ is the past time; Kp^2 is the square of Kp; K_{qm} is the month moving average of Kp; T is the delay of ionosphere relative change amount df over Kp. In this work, set T = 18 h (Gao et al., 2008).

3.3. Neutral winds

The thermospheric wind has effects on the parameters of the ionospheric F layer. According to the well-known vertical ion drift equation (Oyeyemi et al., 2005a),

$$W = U\cos(\theta - D)\cos I\sin I \tag{14}$$

where W is the vertical ion drift velocity, U is the horizontal wind velocity, θ is the geographic azimuth angle. D and I are the magnetic declination and inclination, respectively. In our model, D and I are adopted as the input parameters. D is converted to sine and cosine components of D (DS and DC),

$$DS = \sin\left(\frac{2\pi \times D}{360}\right) \tag{15}$$

$$DC = \cos\left(\frac{2\pi \times D}{360}\right) \tag{16}$$

I is converted to sine component of I (IS),

$$IS = \sin\left(\frac{2\pi \times I}{360}\right) \tag{17}$$

3.4. Geographic coordinates

foF2 has spatial correlation (Cander, 2007). The geographic latitude (LAT) and longitude (LON) are adopted in this model as the geographic coordinates. LAT and LON are also represented by sine and cosine components of LAT ($LATS$ and $LATC$) and LON ($LONS$ and $LONC$) defined as follows:

$$LATS = \sin\left(\frac{2\pi \times LAT}{180}\right) \tag{18}$$

$$LATC = \cos\left(\frac{2\pi \times LAT}{180}\right) \tag{19}$$

$$LONS = \sin\left(\frac{2\pi \times LON}{360}\right) \tag{20}$$

$$LONC = \cos\left(\frac{2\pi \times LON}{360}\right) \tag{21}$$

3.5. Correlation with previous data

The analyses of the F2 layer have shown that, the values of foF2 highly depend on the values in the past hours (Wintoft and Cander, 1999; Oyeyemi et al., 2005a,b, 2006). In this model, we utilize the values of past 5 h as the input vector and measure the variation of foF2 in past 5 h by using first-order deviation, second-order deviation and relative deviation according to the following formula:

$$\Delta_1(h) = f_oF_2(h) - f_oF_2(h-1) \tag{22}$$

$$\Delta_2(h) = \Delta_1(h) - \Delta_1(h-1) \tag{23}$$

$$R\Delta(h) = \Delta_1(h)/f_oF_2(h) \tag{24}$$

3.6. Output parameters

In this study, we concentrate on the forecast of the storm-time foF2 hourly ahead, and the outputs of 1, 3, 6, 12 and 24 h ahead prediction results are demonstrated as output parameters.

3.7. Network configuration

Fig. 1 demonstrates the GA-NN network configuration block diagram. The model includes an input layer with nine inputs, a hidden layer and an output layer with one output vector, as discussed above. In order to achieve the optimal network structure, and to obtain the minimum error difference between the observed and the predicted values of foF2, we have trained several different GA-NN.

The optimum number of hidden layer nodes is highly important that affects the performance of the model. Too many nodes will extend the training time, and even make the network non-convergence; while too little nodes will affect the capacity of information. Hidden layer nodes are difficult to determine. At present, the number of hidden layer nodes are based on experience and experiment method.

Table 2 shows the performance and time of the model with two hidden layers for different nodes. Performance value is evaluated by the mean square error (MSE) when the model training achieves the pre-selected goal of minimum error. As shown in Table 2, the performance of two hidden layers containing 35 and 50 nodes is the best, but the computing time is 108 s. By comparing the results in Table 2, we chose a GA-NN with two hidden layers containing 25 and 35 neurons, respectively.

4. Data set

This work utilizes the hourly foF2 time series from the ionosonde stations in China. Table 3 listed the name and the geographic coordinates of the ionosonde stations for the data set.

In this research, we focus on the foF2 prediction during ionospheric disturbances, especially during geomagnetic storms. Firstly, we define the ionospheric disturbance: if values of foF2 deviate from 15% of the monthly median value, the suspected disturbances start; if foF2 is less than 15% of the month median three hours in succession, the suspected disturbances end; if the duration of the suspected disturbance equals to or is greater than 6 h, we define that the ionospheric disturbance occurs.

The training dataset are from January 1990 to December 2004 except 1995 and 2000. The data of the ionospheric

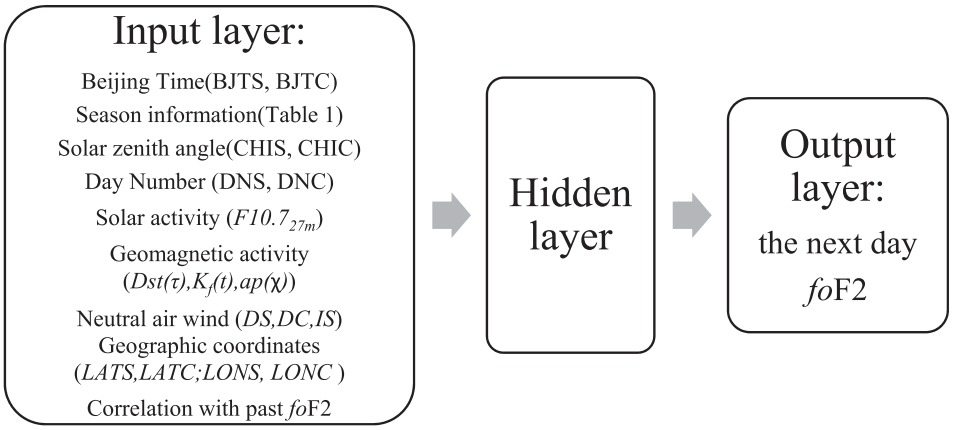

Fig. 1. The block diagram of the GA-NN.

Table 2
The performance and time of the model with two hidden layers for different hidden layer nodes.

Nodes	(25,5)	(25,35)	(25,50)	(35,50)
Performance	0.211	0.181	0.205	0.176
Time/s	3	11	37	108

*f*oF2 in 1995 and 2000 corresponding to solar minimum and maximum, are chosen as representative collections to verify the performance and precision of the GA-NN forecasting model. The training dataset excludes the representative collections to ensure the reliability of test results. The data from the Wuhan (WUH) station are used to examine the capability of single-station forecasting and is not included in this paper (Wang et al., 2013).

To improve the generalization ability of the network, we introduce the normalization expression:

$$y = \frac{x - (1-r)MinValue}{(1+r)MaxValue - (1-r)MinValue} \quad (25)$$

where r = 0.1 is the normalization factor. × and y are the values before and after normalization, respectively. *MaxValue* and *MinValue* are the maximum and minimum value of the samples, respectively. Consequently, the data value will not equal to 0 and 1 after normalization, resulting in a better convergence of the training network.

5. Results

According to the data set mentioned above, we utilize the ionospheric data in the stations HAK, GAZ, CHQ, LHS, LAZ, BEJ, URM, CHC and MAZ in 1995 (solar minimum) and 2000 (solar maximum), to verify the performance of the single station ionospheric disturbance forecasting model by using GA-NN. The root mean square error (RMSE) and the correlation coefficient ρ evaluate the prediction performances and the correlation of the predicted and observed values, respectively.

Table 4 presents the prediction errors of *f*oF2 between the observed and predicted values, which are derived from the single station short-term ionospheric storm forecasting model during the year of solar minimum (1995). As seen in Table 4, the ionospheric *f*oF2 disturbance forecasting model developed in this project works well. For instance, the 1, 3, 6, 12 and 24 h ahead prediction errors RMSE at Beijing (BEJ) station are 0.74 MHz, 0.96 MHz, 0.92 MHz, 0.94 MHz and 0.92 MHz, associated with the correlation coefficient 0.92, 0.87, 0.87, 0.82 and 0.87, respectively.

Table 5 shows the prediction errors of *f*oF2 between the observed and predicted values, which are obtained from the single station short-term ionospheric disturbance forecasting model during the year of solar maximum (2000). It is observed that the performance of the forecasting

Table 3
Geographic coordinates of the ionosonde stations in China.

Station/abbreviation	Geographical Latitude/°N	Geographical Longitude/°E	Magnetic Latitude/°N
Haikou/HAK	20.0	110.3	10.0
Guangzhou/GAZ	23.1	113.3	13.1
Chongqing/CHQ	29.4	106.5	19.4
Lhasa/LHS	29.6	91.1	20.0
Wuhan/WUH	30.6	114.4	20.7
Lanzhou/LAZ	36.0	103.9	26.0
Beijing/BEJ	39.9	116.4	30.0
Urumqi/URM	43.8	87.7	34.3
Changchun/CHC	43.9	125.4	34.3
Manzhouli/MAZ	49.6	117.4	39.7

Table 4
The prediction errors of *fo*F2 between the observed and predicted values during the year of solar minimum (1995).

Station	Prediction errors	Hour(s) ahead				
		1	3	6	12	24
MAZ	RMSE(MHz)	0.55	0.66	0.77	0.91	1.04
	ρ	0.93	0.90	0.85	0.80	0.73
CHC	RMSE(MHz)	0.65	0.84	0.85	0.91	0.94
	ρ	0.92	0.87	0.86	0.84	0.82
URM	RMSE(MHz)	0.69	0.90	1.04	1.10	1.11
	ρ	0.94	0.90	0.87	0.84	0.84
BEJ	RMSE(MHz)	0.74	0.96	0.92	0.94	0.96
	ρ	0.92	0.87	0.87	0.82	0.87
LAZ	RMSE(MHz)	0.82	1.17	1.08	1.05	1.09
	ρ	0.94	0.87	0.89	0.90	0.89
LHS	RMSE(MHz)	0.86	1.14	1.24	1.31	1.14
	ρ	0.95	0.91	0.89	0.87	0.91
CHQ	RMSE(MHz)	1.11	1.57	1.49	1.67	1.77
	ρ	0.93	0.86	0.83	0.83	0.82
GAZ	RMSE(MHz)	1.24	1.80	1.96	1.96	2.09
	ρ	0.93	0.84	0.80	0.80	0.78
HAK	RMSE(MHz)	0.98	1.45	1.61	1.45	1.59
	ρ	0.95	0.89	0.86	0.89	0.88

Table 5
The prediction errors of *fo*F2 between the observed and predicted values during the year of solar maximum (2000).

Station	Prediction errors	Hour(s) ahead				
		1	3	6	12	24
MAZ	RMSE(MHz)	0.59	0.79	1.00	1.20	1.50
	ρ	0.96	0.93	0.90	0.84	0.75
CHC	RMSE(MHz)	0.76	0.92	1.03	1.15	1.52
	ρ	0.94	0.92	0.90	0.89	0.76
URM	RMSE(MHz)	0.70	0.92	1.06	1.29	1.42
	ρ	0.97	0.94	0.92	0.88	0.85
BEJ	RMSE(MHz)	0.77	1.15	1.39	1.43	1.45
	ρ	0.95	0.89	0.85	0.82	0.81
LAZ	RMSE(MHz)	0.85	0.97	1.05	1.16	1.44
	ρ	0.95	0.93	0.92	0.89	0.84
LHS	RMSE(MHz)	0.72	0.79	1.00	1.00	0.93
	ρ	0.98	0.98	0.97	0.97	0.95
CHQ	RMSE(MHz)	1.07	1.49	1.52	1.87	2.15
	ρ	0.95	0.91	0.87	0.85	0.81
GAZ	RMSE(MHz)	1.37	1.87	2.13	2.19	2.32
	ρ	0.94	0.89	0.86	0.85	0.83
HAK	RMSE(MHz)	1.08	1.46	1.68	1.78	1.67
	ρ	0.96	0.92	0.90	0.87	0.90

model in the year of solar maximum is reasonably well. For the ionosonde station Haikou (HAK), the 1, 3, 6, 12 and 24 h ahead prediction errors RMSE are 1.08 MHz, 1.46 MHz, 1.68 MHz, 1.78 MHz and 1.67 MHz, with the correlation coefficient 0.96, 0.92, 0.90, 0.87 and 0.90, respectively.

Figs. 2 and 3 illustrate the bar graph of RMSE differences between the observed and predicted values of *fo*F2 for 1, 3, 6, 12 and 24 h ahead during the low and high (1995 and 2000) solar activity periods. As shown in Figs. 2 and 3, the prediction accuracy of 1 h ahead is superior to the 3, 6, 12 and 24 h ahead. Moreover, the prediction accuracy of 12 and 24 h ahead are generally not as good as 1, 3 and 6 h ahead, which indicate that the longer the predicting hours ahead are, the worse the mode performance is.

As for the ionosonde stations BEJ, LHS and LAZ in Fig. 2 and LHS and HAK in Fig. 3, the prediction accuracy of 24 h ahead is about the same as the 12 h ahead, and even better. This may be roughly explained in the viewpoint of input parameters. We take diurnal variation into account as the input vector in the forecasting model, and the semidiurnal changes are not taken into consideration. But the ionosphere has strong diurnal variations. Thus, the prediction accuracy of 24 h ahead is better than 12 h ahead.

Comparing Fig. 2 with Fig. 3, it is evident that the prediction errors RMSE at middle latitude are generally smaller than those at low latitude in both solar minimum and solar maximum. For example, the prediction accuracy at station CHC is better than that at station GAZ. It may be attributed to the complicated ionosphere variations in the low latitude region, especially during the ionospheric storm, leading to an increase in prediction difficulty and errors.

The predicting results in CHQ, GAZ and HAK are poor comparing to the other stations. The CHQ, GAZ and HAK stations are all in the equatorial anomaly region with high occurrence of local disturbances and instabilities. As shown in Figs. 2 and 3, the predicting results (6 h ahead) in LAZ (poleward of the equatorial anomaly region) are better than those (6 h ahead) in CHQ (in the equatorial anomaly region). In the equatorial anomaly region, the value of *fo*F2 has large variations due to the large changes of the ionospheric and neutral parameters, such as electric fields, resulting in the increase in prediction difficulty.

It is noteworthy that, in Fig. 3, the prediction results at station LHS are better than those at the other stations. On account of seriously data missing at station LHS, the test samples of ionospheric disturbances are smaller. Therefore, the results need further investigation with more data.

Figs. 4 and 5 show the bar graph of RMSE differences between the observed and predicted values of *fo*F2 during the year of solar minimum (1995) and solar maximum (2000), at low latitudes (HAK and GAZ) and middle latitudes (URM and MAZ), respectively. According to Figs. 4 and 5, for the single station short-term ionospheric *fo*F2 disturbance forecasting model, the values of prediction error RMSE in the year of high solar activity (2000) are greater than those in low solar activity (1995). This can be roughly explained that *fo*F2 during the solar maximum is higher than that during the solar minimum, resulting in a greater absolute deviation during the high solar activity period.

On the other hand, at the stations HAK and URM, the prediction errors RMSE 1–3 h ahead are basically the same in the high solar activity and the low solar activity. This may be because that, near or during the ionospheric storm period, the absolute variation of the ionosphere in the low solar activity is possibly larger than that in the high solar

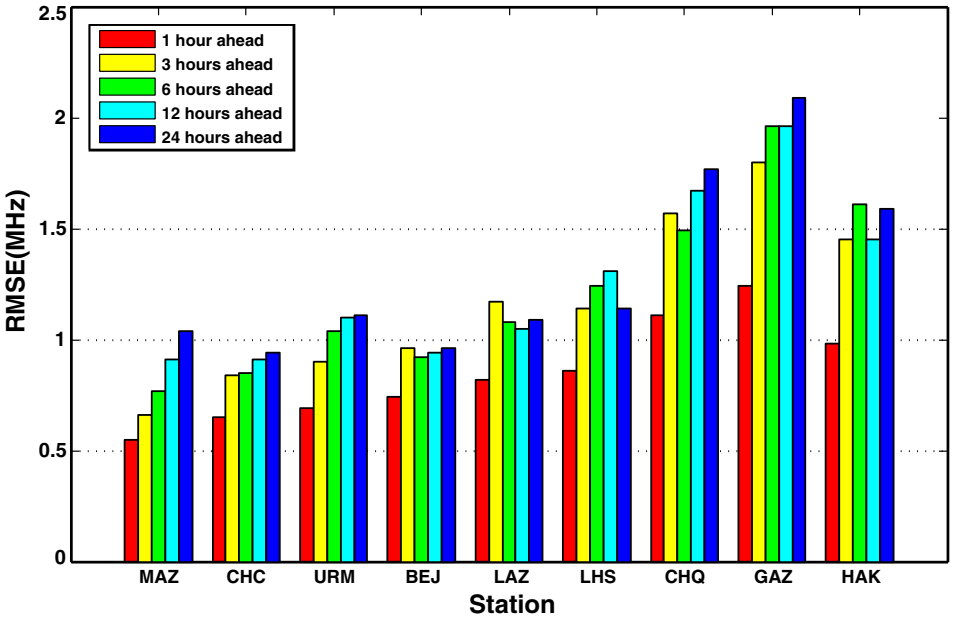

Fig. 2. Bar graph illustrations of RMSE differences between observed and predicted values of *f*oF2 for 1, 3, 6, 12 and 24 h ahead by the GA-NN model during the period of low solar activity (1995).

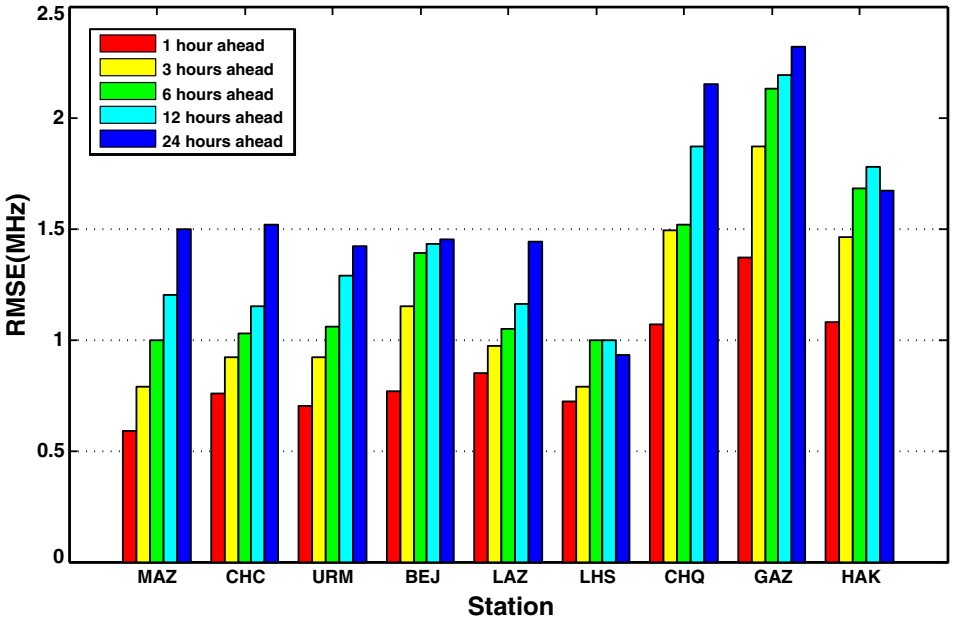

Fig. 3. Bar graph illustrations of RMSE differences between the observed and predicted values of *f*oF2 for 1, 3, 6, 12 and 24 h ahead by the GA-NN model during the period of high solar activity (2000).

activity. The forecasting model in this work is a storm-time model. Therefore, the RMSE 1–3 h ahead are nearly the same, and the RMSE far away from the ionospheric storm period, such as 12 and 24 h ahead are different.

To better revealing the prediction results, the ionospheric storm prediction cases at different stations are given below. The percent deviation r is added to evaluate the prediction performance of the forecasting model. Fig. 6 shows the prediction cases by the single station short-term ionospheric *f*oF2 storm forecasting model at the low latitude stations of HAK and GAZ during the ionospheric *f*oF2 storm in the year of the solar minimum (1995) and the solar maximum (2000). The date and time in each subgraph are the start time of the ionospheric storm. The horizontal axis is the duration of the ionospheric storm, and the vertical axis is the values of *f*oF2. As seen in Fig. 6, the values of *f*oF2 during the high solar activity (2000) period are larger than those in the low solar activity period. The prediction results of 1, 3, 6, 12 and 24 h are satisfactory. For the specific prediction case, take the case occurred at 20:00 BJT on

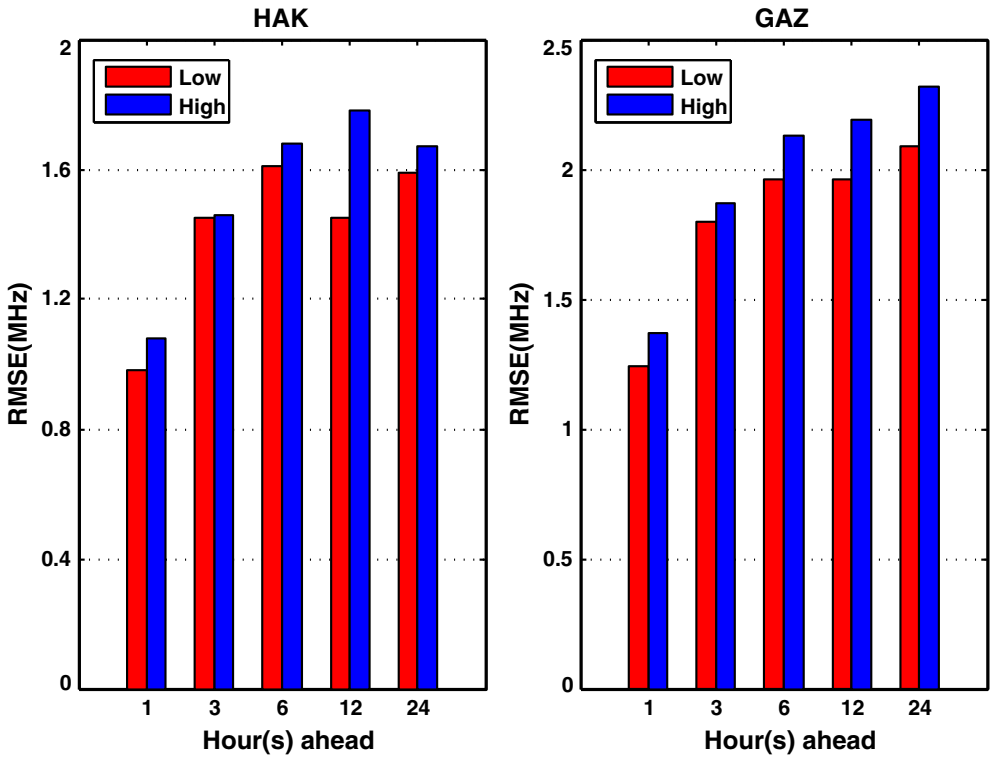

Fig. 4. Bar graph illustrations of RMSE differences between observed and predicted values of *f*oF2 by the GA-NN model during the low and high (1995 and 2000) solar activity periods at low latitudes (HAK and GAZ).

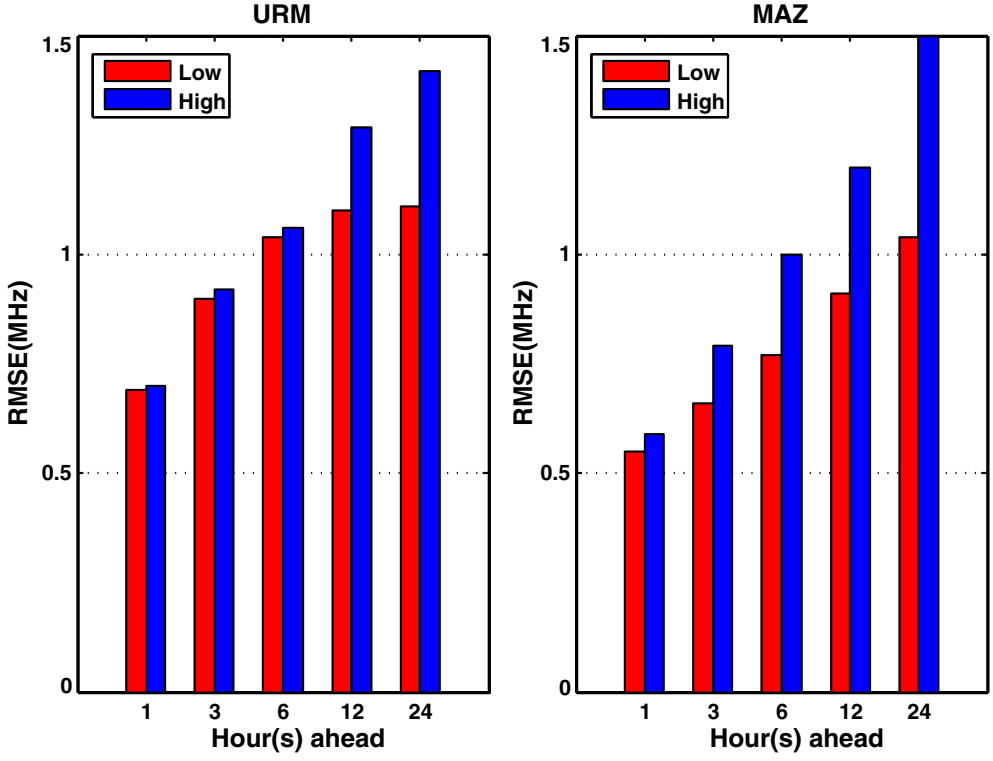

Fig. 5. Bar graph illustrations of RMSE differences between the observed and predicted values of *f*oF2 by the GA-NN model during the low and high (1995 and 2000) solar activity periods at middle latitudes (URM and MAZ).

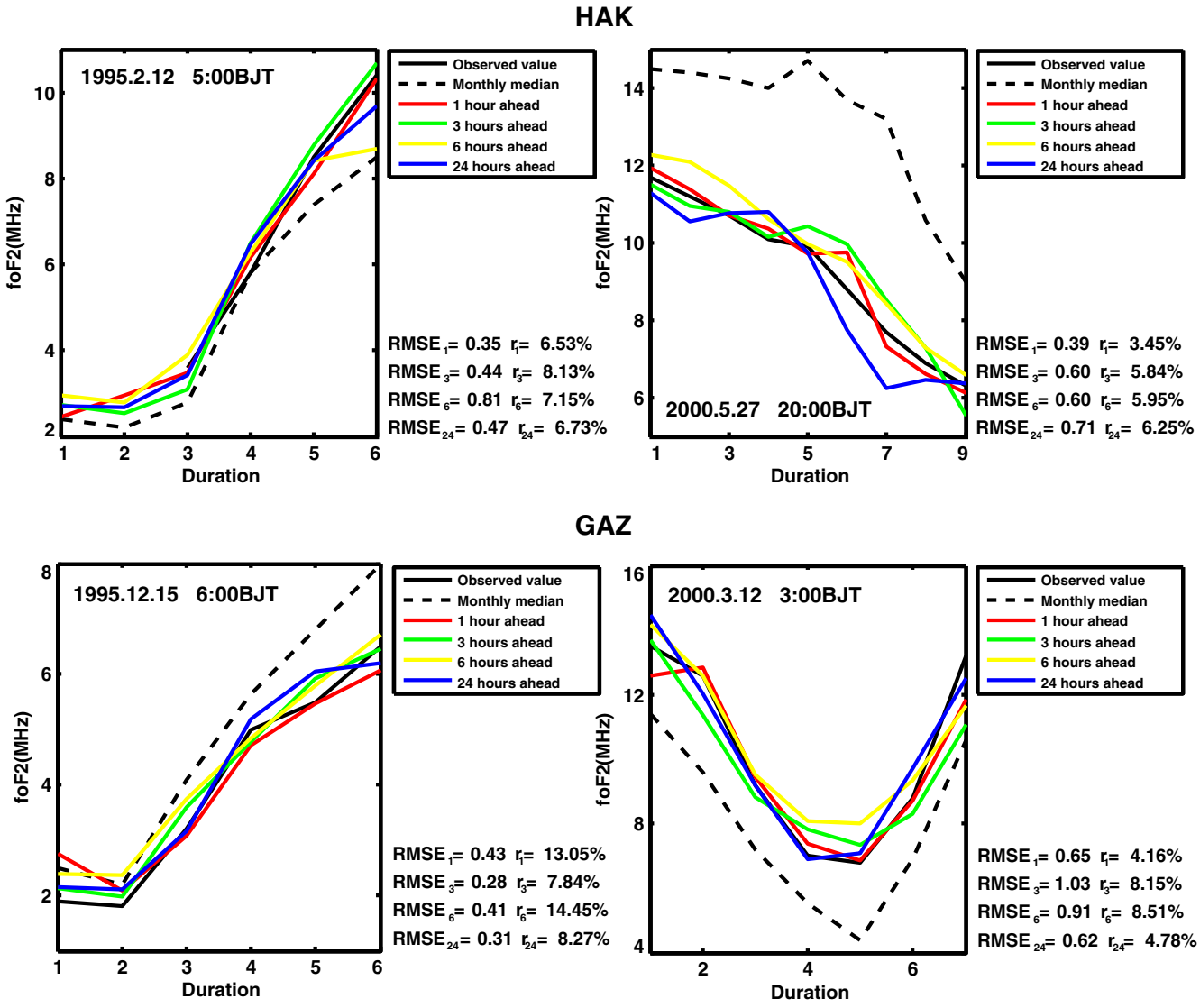

Fig. 6. Comparison of the predicted values and observed values of *f*oF2 by the GA-NN model at low latitudes (HAK and GAZ) during the ionospheric storms in the year of solar minimum (1995) and solar maximum (2000).

May 27, 2000 at the HAK station as an example. It is seen that the observed values of *f*oF2 are far away from the monthly median values, while the value of RMSE is 0.39 MHz with the percent deviation of 3.45% for 1 h ahead prediction.

Fig. 7 illustrates the prediction results at BEJ and MAZ (middle latitude) during ionospheric storms, in the year of the solar minimum (1995) and the solar maximum (2000). In Fig. 7, it is observed that the overall prediction results of single station ionospheric storm forecasting model are acceptable. For the case occurred at 2:00 BJT on April 6, 2000 at the BEJ station, when the observed values of *f*oF2 is far away from the monthly median value, the prediction results show the values of RMSE for the 1 and 24 h predictions 0.13 MHz and 0.23 MHz. For the ionospheric storm case lasting for 18 h, occurred at 17:00 BJT on February 28, 2000 at the MAZ station, the values of RMSE for the 1, 3, 6, 12 and 24 h predictions are relatively small, and the correlations between the predicted values and the observed values of *f*oF2 are consistent.

6. Discussion and conclusions

In this work, a single station short-term ionospheric *f*oF2 disturbance forecasting model has been developed by using GA-NN. The genetic algorithm is adopted to avoid the local minimum effect. Input parameters of this model include the factors associated with geophysical information, solar activity, geomagnetic activity, neutral winds and geographic coordinates. Based on the data of the ionospheric *f*oF2 data in 1995 and 2000, corresponding to the solar minimum and solar maximum, at the stations HAK, GAZ, CHQ, LHS, LAZ, BEJ, URM, CHC and MAZ, the performance of the GA-NN forecasting model

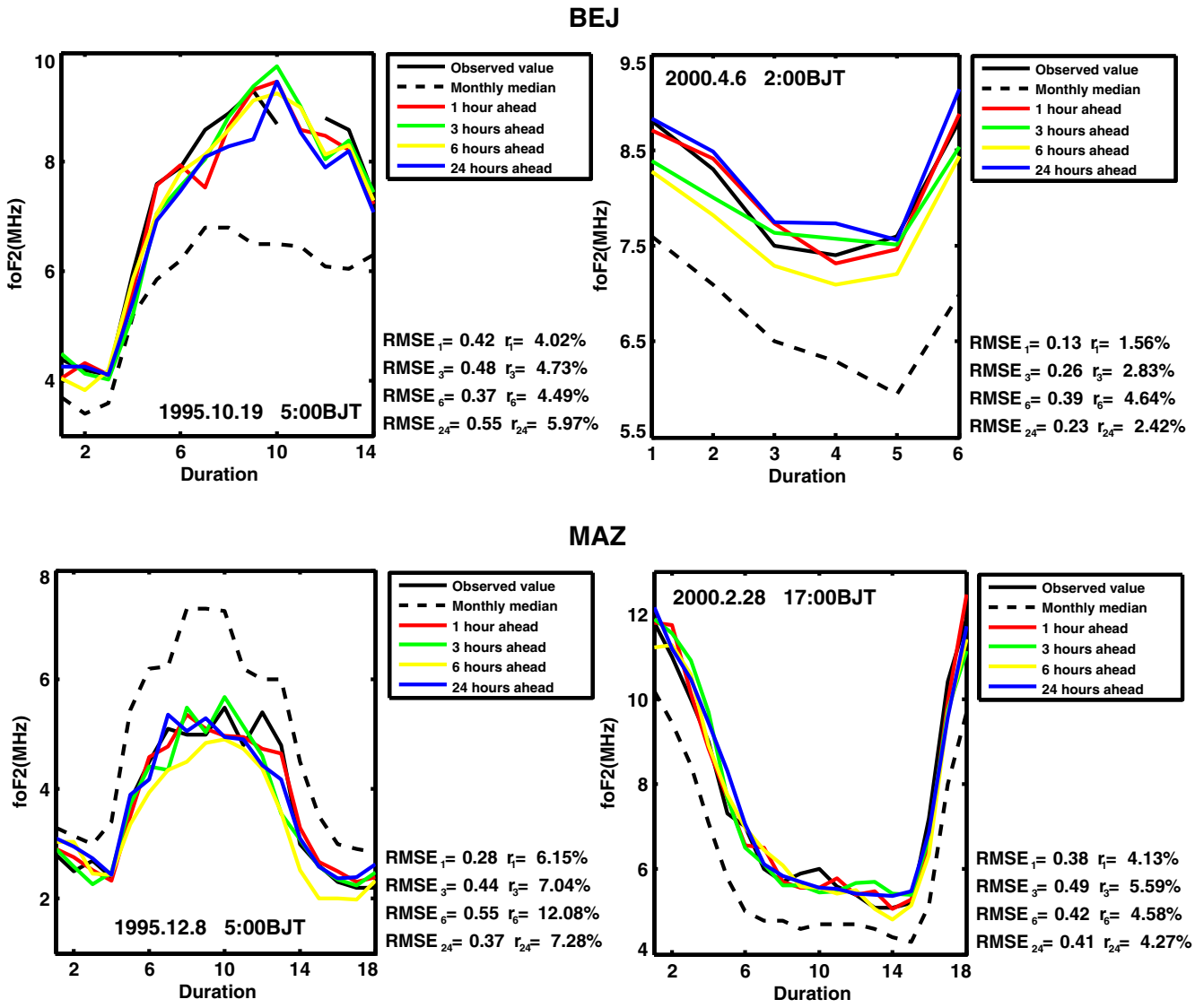

Fig. 7. Comparison of the predicted and observed values of *f*oF2 by the GA-NN model at middle latitudes (BEJ and MAZ) during the ionospheric storms in the year of solar minimum (1995) and solar maximum (2000).

has been investigated and verified. Prediction results reveal that the performance of the ionospheric disturbance forecasting model is reasonably well.

To explore the capability of single-station forecasting, we have used the data from the WUH station to test the GA-NN and NN models. The results have shown that the GA-NN model performs better than the NN model and the International Reference Ionospheric (IRI) model. The results also revealed that all three models can capture the general trend of the observed diurnal and seasonal variability of *f*oF2, and the performance of GA-NN is superior to NN and IRI2007 (Wang et al., 2013).

The prediction RMSE differences, between the observed and predicted values of *f*oF2 for 1, 3, 6, 12 and 24 h ahead predictions by the GA-NN model, during the low and high (1995 and 2000) solar activity periods, show that the prediction errors RMSE at middle latitude are generally less than that at low latitudes both in the year of the solar minimum and the solar maximum. The comparison results also show that the prediction accuracy of 1 h ahead is better compared with 3, 6, 12 and 24 h ahead. The performance of the prediction tends to be worse as the predicting ahead time increases. However, some stations show that the prediction accuracy of 24 h ahead is as good as or even better than 12 h ahead. This results suggest that our model can be affected by semidiurnal changes of the ionosphere, and the semidiurnal variation should be taken into account in the future work. Comparisons of RMSE differences during the year of solar minimum (1995) and solar maximum (2000) indicate that, due to the higher values of *f*oF2 during the high solar activity period (2000), the prediction errors RMSE in the year of the high solar activity (2000) are larger than those in low solar activity (1995).

To better explain the prediction performance of the model, the ionospheric storm prediction cases at different stations are demonstrated. The prediction results for 1, 3,

6 and 24 h ahead are very promising. For the two specific cases, of which the observed values of *fo*F2 far away from the monthly median value and the ionospheric storm lasting for 18 h, the prediction errors are small. The correlations between the predicted values and the observed values are consistent.

Different combination of input variables leads to different model performance. Comparing the different combination of input variables for the GA-NN model to find the optimum choice of the input parameters is very important, and will be the focus in the future work.

Moreover, the *fo*F2 is highly variable in both time and space during geomagnetic storms, it is very difficult to predict exactly *fo*F2 variations. In this work, we only use the input parameters mentioned in Section 3. However, the *fo*F2 variations depend on many parameters such as neutral density, disturbance dynamo winds and prompt penetration electric fields or drifts. Also, the information of the solar wind and IMF *Bz* values, type of CME events such as CME or ICMEs are also very important parameters that affect *fo*F2 variations. The effects of Joule heating on the prediction of *fo*F2 variations during storms should also be included. The parameters aforementioned require further investigations in our future studies.

Acknowledgement

This work was carried out with the financial support from the China Earthquake Administration (No. 201008007). We acknowledge the use of data from the Chinese Meridian Project. This work was supported by the National Natural Science Foundation of China (NSFC grant No. 41204111, 41574146, 41774162).

References

Abdu, M.A., Batista, I.S., Walker, G.O., Walker, J.H.A., Sobral, N.B., Trivedi, E.R., de Paula, 1995. Equatorial ionospheric electric fields during magnetospheric disturbances: local time/longitude dependences from recent EITS campaigns. J. Atmos. Terr. Phys. 57 (10), 1065–1083. https://doi.org/10.1016/0021-9169(94)00123-6.

Altinay, O., Tulunay, E., Tulunay, Y., 1997. Forecasting of ionospheric critical frequency using neural network. Geophys. Res. Lett. 24, 1467–1470. https://doi.org/10.1029/97GL01381.

Apostolov, E.M., Altadill, D., Todorova, M., 2004. The 22-year cycle in the geomagnetic 27-day recurrences reflecting on the F2-layer ionization. Ann. Geophys. 22, 1171–1176. https://doi.org/10.5194/angeo-22-1171-2004.

Appleton, E.V., Naismith, R., Ingram, L.J., 1937. British radio observations during the second international polar year 1932–1933. Philos. Trans. Roy. Sec. A236, 191–259. https://doi.org/10.1098/rsta.1937.0002.

Ban, P.P., Sun, S.J., Chen, C., Zhao, Z., 2011. Forecasting of low-latitude storm-time ionospheric *fo*F2 using support vector machine. Radio Sci. 46, RS6008. https://doi.org/10.1029/2010RS004633.

Bilitza, D., 2002. Ionospheric models for radio propagation studies. In: Stone, W.R. (Ed.), The Review of Radio Science 1999–2002: Advances in 3G Mobile Communications, Cryptography and Computer Security, EMC for Integrated Circuits, Remote Sensing, Radio Astronomy and More. IEEE Press, Piscataway, N. Y, pp. 625–680.

Buonsanto, M.J., 1999. Ionospheric storms-a review. Space Sci. Rev. 88 (3), 63–601. https://doi.org/10.1023/a:1005107532631.

Cander, L.R., Mihajlovic, S.J., 2005. Ionospheric spatial and temporal variations during the 29–31 October 2003 storm. J. Atmos. Sol. Terr. Phys. 67 (12), 1118–1128. https://doi.org/10.1016/j.jastp.2005.02.020.

Cander, L.R., 2007. Spatial correlation of foF2 and vTEC under quiet and disturbed ionospheric conditions: a case study. Acta Geophys. 55 (3), 410–423. https://doi.org/10.2478/s11600-007-0011-9.

Francis, N.M., Cannon, P.S., Brown, A.G., 2000. Nonlinear prediction of the ionospheric parameter *f*oF2 on hourly, daily, and monthly timescales. J. Geophys. Res. 105 (A6), 12839–12849. https://doi.org/10.1029/2000JA900005.

Gao, Q., Liu, L.B., Zhao, B.Q., Wan, W.X., Zhang, M.L., Ning, B.Q., 2008. Statistical study of the storm effects in middle and low latitude ionosphere in the East-Asian sector. Chin. J. Geophys. 51 (3), 626–634. https://doi.org/10.1002/cjg2.1234.

Goldberg, M.B., Gufeld, I.L., Rozhnoy, A.A., Marenko, V.F., Yampolsky, V.S., Ponomarev, E.A., 1989. Study of seismic influence on the ionosphere by super long-wave probing of the Earth-ionosphere waveguide. Phys. Earth Planet. In. 57 (1–2), 64–67. https://doi.org/10.1016/0031-9201(89)90214-8.

Goodman, J.M., 1992. HF Communications Science and Technology. Van Nostrand Reinhold, New York.

Hebden, S.R., Robinson, T.R., Wright, D.M., Yeoman, T., Raita, T., Singer, T.B., 2005. Observations by the CUTLASS radar, HF Doppler, oblique ionospheric sounding, and TEC from GPS during a magnetic storm. Ann. Geophys. 23 (5), 1697–1709. https://doi.org/10.5194/angeo-23-1711-2005.

Kirby, S.S., Gilliland, T.R., Smith, N., Reymer, S.E., 1936. The ionosphere, solar eclipse and magnetic storm. Phys. Rev. 50, 258–259. https://doi.org/10.1103/PhysRev. 50.258.

Kumluca, A., Tulunay, E., Topalli, I., Tulunay, Y., 1999. Temporal and spatial forecasting of ionospheric critical frequency using neural networks. Radio Sci. 34 (6), 1497–1506. https://doi.org/10.1029/1999rs900070.

Kutiev, I., Muhtarov, P., 2001. Modeling of mid-latitude F region response to geomagnetic cativity. J. Geophys. Res. 106 (A8), 15501–15509. https://doi.org/10.1029/2001JA900018.

Lampinen, J., 2003. Cam shape optimization by genetic algorithm. Comput. Aided Des. 35 (8), 727–737. https://doi.org/10.1016/S0010-4485(03)00004-6.

Liang, M.C., Li, K.F., Shia, R.L., Yung, Y.L., 2008. Short-period solar cycle signals in the ionosphere observed by FORMOSAT-3/COSMIC. Geophys. Res. Lett. 35 (15), 1–4. https://doi.org/10.1029/2008GL034433.

Montana, D., Davis, L., 1989. Training feedforward neural networks using genetic algorithms. In: Proceedings of the Eleventh International Joint Conference on Artificial Intelligence. Morgan Kaufmann, San Mateo, CA, pp. 762–767.

Nakamura, M.I., Maruyama, T., Shidama, Y., 2007. Using a neural network to make operational forecasts of ionospheric variations and storms at Kokubunji. Earth Planets Space 59 (12), 1231–1239. https://doi.org/10.1186/BF03352071.

Oyeyemi, E.O., Poole, A.W.V., 2004. Towards the development of a new global *fo*F2 model using neural networks. Adv. Space Res. 34, 1966–1972. https://doi.org/10.1016/j.asr.2004.06.010.

Oyeyemi, E.O., Poole, A.W.V., McKinnell, L.A., 2005a. On the global model for *fo*F2 using neural networks. Radio Sci. 40 (6), 1–15. https://doi.org/10.1029/2004RS003223.

Oyeyemi, E.O., Poole, A.W.V., McKinnell, L.A., 2005b. On the global short-term forecasting of the ionospheric critical frequency foF2 up to 5 hours in advance using neural networks. Radio Sci. 40 (6), 5347–5356. https://doi.org/10.1029/2004RS003239.

Oyeyemi, E.O., Mckinnell, L.A., Poole, A.W.V., 2006. Near-real time *fo*F2 predictions using neural networks. J. Atmos. Sol. Terr. Phys. 68 (16), 1807–1818. https://doi.org/10.1016/j.jastp.2006.07.002.

Poole, A.W.V., Mckinnell, L.A., 2000. On the predictability of *fo*F2 using neural networks. Radio Sci. 35 (1), 225–234. https://doi.org/10.1029/1999RS900105.

Renner, G., Ekárt, A., 2003. Genetic algorithms in computer aided design. Comput. Aided Des. 35 (8), 709–726. https://doi.org/10.1016/s0010-4485(03)00003-4.

Tulunay, Y., Tulunay, E., Senalp, E.T., 2004. The neural network technique-2:an ionospheric example illustrating its application. Adv. Space Res. 33 (6), 988–992. https://doi.org/10.1016/j.asr.2003.06.015.

Wang, X.M., Shi, J.K., Wang, G., Zherebtsov, G.A., Pirog, O.M., 2008. Responses of ionospheric foF2 to geomagnetic activities in Hainan. Adv. Space Res. 41 (4), 556–561. https://doi.org/10.1016/j.asr.2007.04.097.

Wang, R., Zhou, C., Deng, Z., Ni, B., Zhao, Z., 2013. Predicting *f*oF2 in the China region using the neural networks improved by the genetic algorithm. J. Atmos. Sol. Terr. Phys. 92 (3), 7–17. https://doi.org/10.1016/j.jastp.2012.09.010.

Williscroft, L.A., Poole, A., 1996. Neural networks *f*oF2 sunspot number and magnetic activity. Geophys. Res. Lett. 23 (24), 3659–3662. https://doi.org/10.1029/96GL03472.

Wintoft, P., Cander, L.R., 1999. Short-term prediction of foF2 using time-delay neural network. Phys. Chem. Earth C Sol. Terr. Planet. Sci. 24 (4), 343–347. https://doi.org/10.1016/S1464-1917(99)00009-4.

Wintoft, P., Cander, L.R., 2000. Ionospheric *f*oF2 storm forecasting using neural networks. Phys. Chem. Earth C Sol. Terr. Planet. Sci. 25 (4), 267–273. https://doi.org/10.1016/S1464-1917(00)00015-5.

Zhou, C., Wang, R., Lou, W., 2013. Preliminary investigation of real-time mapping of *f*oF2 in northern China based on oblique ionosonde data. J. Geophys. Res. 118 (5), 2536–2544. https://doi.org/10.1002/jgra.50262.

Zolesi, B., Cander, L.R., 2000. Evolution of the ionospheric mapping and modelling during the last four decades. Fisica De La Tierra 12, 127–154 https://dialnet.unirioja.es/servlet/articulo?codigo=124592.